Pharmacokinetics of Interstitial Delivery of Carmustine, 4-Hydroperoxycyclophosphamide, and Paclitaxel from a Biodegradable Polymer Implant in the Monkey Brain

Article *in* Cancer Research · March 1998

Source: PubMed

CITATIONS
266

READS
219

9 authors, including:

Lawrence Fung
Stanford University
72 PUBLICATIONS **2,299** CITATIONS
SEE PROFILE

Matthew G Ewend
University of North Carolina at Chapel Hill
147 PUBLICATIONS **7,277** CITATIONS
SEE PROFILE

William Mark Saltzman
Yale University
423 PUBLICATIONS **28,173** CITATIONS
SEE PROFILE

Pharmacokinetics of Interstitial Delivery of Carmustine, 4-Hydroperoxycyclophosphamide, and Paclitaxel from a Biodegradable Polymer Implant in the Monkey Brain

Lawrence K. Fung, Matthew G. Ewend, Allen Sills, et al.

Cancer Res 1998;58:672-684. Published online February 1, 1998.

[CANCER RESEARCH 58, 672–684, February 15, 1998]

Pharmacokinetics of Interstitial Delivery of Carmustine, 4-Hydroperoxycyclophosphamide, and Paclitaxel from a Biodegradable Polymer Implant in the Monkey Brain[1]

Lawrence K. Fung, Matthew G. Ewend,[2] Allen Sills,[2] Eric P. Sipos,[2] Reid Thompson,[2] Mark Watts, O. Michael Colvin, Henry Brem,[3] and W. Mark Saltzman[4]

School of Chemical Engineering, Cornell University, Ithaca, New York 14853 [L. K. F., W. M. S.]; Departments of Neurosurgery [M. G. E., A. S., E. P. S., R. T., M. W., H. B.] and Oncology [H. B.], The Johns Hopkins School of Medicine, Baltimore, Maryland 21287; and Comprehensive Cancer Center, Duke University Medical Center, Durham, North Carolina 27710 [O. M. C.]

ABSTRACT

Polymeric interstitial chemotherapy increases survival of humans with recurrent gliomas and animals with transplanted tumors in the brain, but the relationship between rates of drug release from polymer implants and drug concentration in brain tissue is unknown. This work presents a pharmacokinetic framework for application of this new modality of chemotherapy delivery in primates. Either [^{3}H]carmustine, 4-hydroperoxycyclophosphamide (4-HC), or paclitaxel was encapsulated in a polyanhydride pellet (28–41 μCi/animal, 40 mg/animal), which was implanted intracranially in cynomolgus monkeys (*Macaca fascicularis*); (n = 17) for up to 30 days. Drug concentrations in the brain, blood, and cerebrospinal fluid were measured by quantitative autoradiography, TLC, and scintillation counting. High drug concentrations (0.5–3.5 mM for carmustine, 0.3–0.4 mM for 4-HC, and 0.2–1.0 mM for paclitaxel) were measured within the first 3 mm from the polymer implant; significant (0.4 μM for carmustine, 3 μM for 4-HC, and 0.6 μM for paclitaxel) concentrations were measured up to ~5 cm from the implant as long as 30 days after implantation. Pharmacokinetic analysis indicated that tissue exposure to carmustine area under concentration-time curve achieved by polymeric delivery was 4–1200 times higher than that produced by i.v. administration of a higher dose.

INTRODUCTION

Intracerebral chemotherapy delivery by polymer implants increases survival of humans with recurrent malignant gliomas (1, 2) and of animals with transplanted gliomas (3–10). Drug-loaded polymer pellets implanted intracranially bypass the BBB[5] and release drug molecules locally in the brain in a sustained fashion. Malignant gliomas are known to recur within a few cm from the tumor excision site (11–13); thus, the effectiveness of the drug delivered by polymers is dependent on whether drug molecules can be transported a sufficient distance from the implantation site. Existing knowledge regarding the local distribution and pharmacokinetics of anticancer agents delivered by polymer implants is largely based on studies in rodents (6, 14–18). To improve our understanding of the pharmacokinetic basis of intracerebral polymeric chemotherapy in humans, we implanted biodegradable polyanhydride pellets containing carmustine [1,3-bis(2-chloroethyl)-1-nitrosourea], 4-HC, or paclitaxel into the brains of cynomolgus monkeys and measured drug concentrations in the brain, blood, and CSF during the subsequent 30-day period. Using a mathematical model, the experimental data were used to evaluate the mechanisms of transport (diffusion and convection), elimination (degradation and transcapillary action), and binding of these agents in the primate brain.

MATERIALS AND METHODS

Animals. Seventeen adult male cynomolgus monkeys (*Macaca fascicularis*), each weighing 4–5 kg, were obtained from the Primate Information Clearinghouse, Whitesand Research Center (Holloman Air Force Base, NM). The monkeys were caged individually with free access to Agway Prolab Primate 18 Formula and Baltimore, MD, city water. The monkeys were randomly assigned to one of the three experimental groups, with each animal in a group receiving a PCPP-SA polymer disc loaded with either carmustine, 4-HC, or paclitaxel. Following implantation of the polymer disc, animals in the carmustine group were sacrificed at day 1 (n = 2), 3 (n = 1), 5 (n = 1), 7 (n = 1), 14 (n = 1), or 30 (n = 1); animals in both the 4-HC and paclitaxel groups were sacrificed at day 1 (n = 2), 3 (n = 2), or 7 (n = 1).

Materials. Carmustine was provided by the Drug Synthesis and Chemistry Branch, Developmental Therapeutics Program, Division of Cancer Treatment, National Cancer Institute and purchased from Bristol-Myers Squibb Company (Princeton, NJ). [^{3}H]Carmustine (35 μCi/mg and 1 mCi/mg) was synthesized and purchased from Amersham International (Buckinghamshire, England). Paclitaxel and [^{3}H]paclitaxel (0.5 mCi/ml toluene) were provided kindly by National Cancer Institute. 4-HC was a gift from Nova Pharmaceutical Corp. (Baltimore, MD). [^{3}H]4-HC (8.0 μCi/mg) was synthesized according to a published procedure (19). In brief, unlabeled materials were used to generate the intermediate 3-butenyl *N,N*-bis(2-chloroethyl)phosphorodiamidate, which was then sent to SibTech, Inc. (Tenafly, NJ) for random incorporation of ^{3}H. The resultant [^{3}H]phosphorodiamidate (greater than 35 μCi/mg) was ozonated to give 4-HC with random incorporation of ^{3}H (8 μCi/mg). PCPP-SA (20:80 w/w ratio) polymer was kindly provided by Guilford Pharmaceuticals, Inc. (Baltimore, MD). Ketamine hydrochloride and sodium pentobarbital were purchased from Parke-Davis (Morris Plains, NJ) and Ampro Pharmaceutical (Arcadia, CA), respectively.

Fabrication of Drug-loaded Polymer Discs. Carmustine, 4-HC, and paclitaxel were encapsulated individually in PCPP-SA polymer discs by solvent evaporation, as follows. Typically, 200 mg of nonradioactive drug (carmustine, 4-HC, or paclitaxel), the corresponding tritiated analogue of the drug [approximately 205 (or 140) μCi for carmustine, 145 μCi for 4-HC, and 200 μCi for paclitaxel], and 800 mg of PCPP-SA copolymer were dissolved in ~8 ml of methylene chloride at room temperature. The solution was then transferred to a Petri dish, and the methylene chloride was evaporated in a vacuum desiccator. Approximately 200 mg of the dried product were compressed at ~8000 p.s.i. for 5 s or at ~3000 p.s.i. for ~17 s in a mold to form a 200-mg polymer

Received 7/22/97; accepted 12/12/97.

The costs of publication of this article were defrayed in part by the payment of page charges. This article must therefore be hereby marked *advertisement* in accordance with 18 U.S.C. Section 1734 solely to indicate this fact.

[1] This study was supported by NIH Grant U01-CA52857 and was presented in part at the 87th Annual Meeting of the American Association for Cancer Research (Washington, DC) in 1995 and the First Scientific Meeting of the Society for Neuro-Oncology (Santa Fe, NM) in 1996.

[2] Recipients of the NIH National Research Service Award CA-09574.

[3] Guilford Pharmaceuticals, Inc. provided partial funding for the study described in this paper. The Johns Hopkins University and H. B. will receive a share of sales royalties from Guilford, and they own Guilford stock, the sale of which is subject to certain restrictions under University policy. H. B. is also a consultant to Guilford, and Guilford has provided a gift for research in H. B.'s laboratory. The terms of this arrangement are being managed by the University in accordance with its conflict of interest policies.

[4] To whom requests for reprints should be addressed, at 120 Olin Hall, School of Chemical Engineering, Cornell University, Ithaca, NY 14853. E-mail: saltzman@cheme.cornell.edu.

[5] The abbreviations used are: BBB, blood-brain barrier; AUC, area under the concentration-time curve; CM, cell membrane; CSF, cerebrospinal fluid; ECS, extracellular space; 4-HC, 4-hydroperoxycyclophosphamide; ICS, intracellular space; PCPP-SA, poly[bis-(*p*-carboxyphenoxy)propane-sebacic acid].

disc (10 mm in diameter and 1 mm in thickness). The [^{3}H]carmustine, [^{3}H]4-HC, and [^{3}H]paclitaxel discs contained about 41 (or 28), 29, and 40 μCi, respectively, with ~40 mg of the corresponding unlabeled agents. The discs were sterilized by exposure to γ-irradiation from a cesium source (2.3–2.5 Mrad for 747 min), and kept in sterile vials at −40°C until the day of surgery.

***In Vitro* Release Study.** The release of [^{3}H]carmustine (n = 2), [^{3}H]4-HC (n = 1), and [^{3}H]paclitaxel (n = 2) from PCPP-SA discs was monitored during incubation in 20 ml of PBS [120 mM NaCl, 2.7 mM KCl, and 10 mM phosphate buffer (pH 7.4)] under gentle agitation at 37°C. At specific times following immersion, the buffer solution was replaced with fresh solution, and the radioactivity in the removed solution was determined by scintillation counting.

Surgical Implantation of Polymer Disc in Monkey Brain. Monkeys were anesthetized after a 12-h fast (without restricting water consumption) with an i.m. injection of ketamine hydrochloride (10 mg/kg), then transferred to the operating suite. A catheter was inserted into a calf vein for continuous i.v. infusion of Ringer's lactate solution throughout the procedure. The monkeys were intubated endotracheally under direct vision and maintained on halothane inhalational anesthesia with continuous cardiac and respiratory monitoring. Each monkey was positioned prone, and all limbs were secured. The scalp over the operative site was shaved, disinfected, and draped in sterile fashion. A small C-shaped incision extending from the left superior orbital ridge posteriorly and inferiorly was made, and scalp bleeding was controlled with electrocautery. The underlying temporalis fascia and muscle were then divided with electrocautery. A high-speed air drill was used to create a 1.0 × 1.5-cm ovoid craniectomy in the left frontal bone extending from the supraorbital ridge posteriorly. A 1.5-cm dural incision was made, exposing the left frontal lobe. A small linear corticotomy was made by using bipolar cautery and gentle suction. Once hemostasis was achieved, a single sterile 200-mg disc (20:80 PCPP-SA with 20% carmustine, 4-HC, or paclitaxel by weight) was inserted into the cortical defect until it was completely beneath the cortical surface. The sterile field was irrigated and, once it was determined that there was no residual bleeding, a rectangular piece of Gelfoam was placed to fit the craniectomy defect. The temporalis muscle fascia was closed with a running 3.0 Vicryl suture, and the scalp was closed with interrupted 3.0 Prolene sutures. The anesthetic was discontinued, and each of the animals was extubated uneventfully. Once the monitors were disconnected and the i.v. catheters were removed, the animals were transported back to the housing facility and observed during recovery from anesthesia.

Blood and CSF Sampling and Analysis. At 6 h and 1, 3, 7, 10, 14, 21, and 30 days following polymer implantation, three animals with carmustine-impregnated polymer pellets implanted were anesthetized by i.m. injection of ketamine hydrochloride. Blood was collected from the femoral vein into an EDTA-coated tube. CSF was collected by cervical or lumbar puncture into a sterile glass tube. Both blood and CSF were placed on ice upon sampling and stored at 0°C until assay. Blood and CSF samples were then assayed as follows. One ml of each sample was placed in a polypropylene tube, and 3 ml of chilled diethyl ether were added. The tube was then capped and shaken gently for 10 min. The diethyl ether, which contained the extracted carmustine and its metabolites, was then spotted on a TLC sheet (Aldrich, Milwaukee, WI). The chromatogram was developed with chloroform. Carmustine spots were then located under an UV lamp. The portion of the chromatogram containing carmustine was separated, and the ^{3}H activity of each portion of the chromatogram was measured by scintillation counting. Two hundred ml of the residual blood sample were mixed with 1 ml of a 1:1 mixture of Soluene 350 (Packard, Meriden, CT) and isopropanol with gentle agitation in a scintillation vial and then incubated at 40°C for 15–30 min. After the samples were cooled to ambient temperature, 0.5 ml of hydrogen peroxide was added dropwise while the solution was swirled to discolor it. This mixture was left at room temperature for 15–30 min, after which it was incubated for 15 min at 40°C to decompose the excessive hydrogen peroxide. After cooling, 10 ml of Hionic-Fluor (Packard) were added to the resulting solution for scintillation counting. Residual CSF samples were mixed with 5 ml of scintillation mixture for liquid scintillation counting.

Monkey Necropsy. Animals were sacrificed at the scheduled intervals. Immediately before the sacrifice of each animal, blood was drawn from the femoral vein, and CSF was obtained by lumbar puncture. Each blood sample was treated using the procedure for the residual blood samples described above. Fifty ml of CSF were obtained from each sample and mixed with 5 ml of scintillation mixture for liquid scintillation counting. The animals were sacrificed by i.v. injection of ~6 ml of sodium pentobarbital. The brain was quickly removed and divided into eight segments, four from each hemisphere (Fig. 1). The brain segments were quickly weighed, frozen on dry ice, and stored at −80°C.

Regional Drug Distribution. Frozen brain segments were mounted on a specimen holder with OCT embedding medium (Miles, Inc., Elkhart, IN) and sectioned into 20- or 60-μm coronal slices using a microtome cryostat (Microm, Heidelberg, Germany) at −20°C. Every 10th section was collected, minced on a Petri dish over dry ice, and transferred to a preweighed Eppendorf tube or glass vial. The radioactivity of part of the minced tissue sample was measured by scintillation counting following tissue digestion (described in procedure A, below); for the residual tissue sample, the drug was extracted, and the percentage of radioactivity representing the intact drug was obtained by TLC and scintillation counting (described in procedure B, below).

In procedure A, approximately 2 ml of NCS tissue solubilizer (Amersham Corp., Arlington Heights, IL), 60 μl of 97% acetic acid, and 150 μl of deionized water were added to a preweighed portion of a minced brain tissue sample; in some cases, 1.5 ml of Soluene 350 and 0.4 ml of deionized water were added to the brain tissue sample. The samples were kept at 50°C overnight. The digested sample was allowed to cool, and 5 ml of scintillation mixture were added to 200 μl of the resulting solution for liquid scintillation counting. When Soluene 350 was used instead of NCS tissue solubilizer, 10 ml of scintillation mixture were added directly to a digested sample. The distribution of tritium in sections obtained on the anteroposterior axis of the monkey brains was determined from the relative position, total tritium activity, and weight of the coronal slice.

In procedure B, chemotherapeutic agents in the minced brain tissue samples were extracted with absolute ethanol, and the residual tissue was separated by centrifugation. The ethanol extract was sprayed dry with nitrogen and redis-

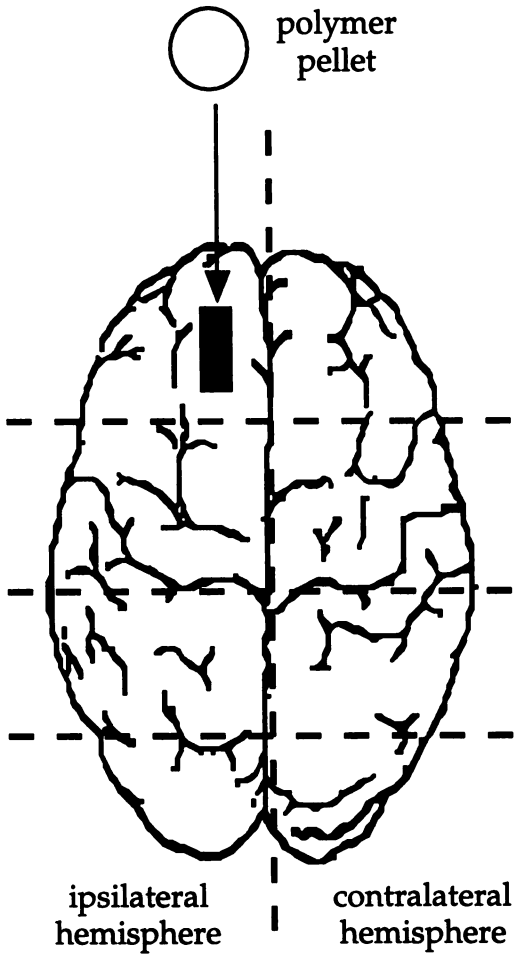

Fig. 1. Division of the monkey brain at necropsy. Each monkey brain was divided into eight segments, four in each hemisphere. The polymer disc was contained in the most anterior segment in the left hemisphere.

Fig. 2. Orientations of scans on autoradiographic images for local concentration measurements in coronal sections. Concentration profiles were scanned perpendicularly from the flat surfaces of the polymer disc to the edge of the brain.

solved in ~20 μl of absolute ethanol. The extract was then spotted on a TLC sheet, which was developed with chloroform for carmustine, with a 1:1 mixture of acetone and chloroform for 4-HC, or with a 1:3 mixture of acetone and chloroform for paclitaxel. Carmustine and paclitaxel spots were localized with fluorescence under UV light, whereas 4-HC spots were localized with iodine vapor from sublimized iodine crystals. The portion of the TLC sheet containing the authentic compound (carmustine, 4-HC, or paclitaxel) was separated from the rest of the TLC sheet. The activities of both portions of the chromatogram were measured by scintillation counting. The residual tissue after extraction was digested by 1 ml of NCS tissue solubilizer, 30 μl of 97% acetic acid, and 75 μl of deionized water. The mixture was kept at 50°C for 24 h, and the tritium activity within this insoluble fraction of tissue was measured by scintillation counting.

Local Drug Distribution by Quantitative Autoradiography. Each frozen brain segment that contained a polymer disc was mounted on a specimen holder with OCT embedding medium and cut into 20-μm coronal sections using a cryomicrotome at −20°C. Every 20th section was collected on a glass slide, so that the total distance between collected sections was 400 μm, and the slides were placed in an X-ray cassette that contained ^{3}H-sensitive autoradiography film [LKB Ultrofilm from Leica (Deerfield, IL) or Hyperfilm from Amersham Corp.). In addition to the brain sections, a commercially prepared tritium microscale (Amersham Corp.) with eight different premeasured activities was placed within the cassette. The autoradiography film was exposed for 2–3 weeks at room temperature. The film was then developed for 5 min at about 22°C (D-19 developer); immersed for 30 s in a stop bath (for Leica Ultrofilms only), 5 min in fixer, and 20 min in filtered flowing water at 22°C; and allowed to dry (all solutions from Kodak).

Previously developed autoradiographic films were placed on a light box and digitized to produce digital images that were 512 × 512 pixels with 256 gray levels. The tritium activity at each pixel location was determined by comparing the pixel absorbance to a standard curve obtained from digital images of tritium-labeled standards, which were reproduced on each film and digitized identically to the brain sections. The freeware program NIH-Image (written by Wayne Rasband; available by anonymous FTP from zippy.nimh.nih.gov) was used to measure concentration profiles from individual digital images; concentration profiles at the implant site were determined directly from digital images by scanning the image from the edge of the polymer to the periphery of the brain section (Fig. 2). Local concentrations obtained by this method were in radioactivity units (nCi/mg). To convert radioactivity to molar units of active drug, the fraction of radioactivity representing intact drug in coronal sections closest to the polymer discs was determined by TLC and scintillation counting, as described above. Concentrations of active drug were obtained by using the following formula: concentration in mM = (radioactivity in nCi/mg tissue) × (density of tissue in g/cm^3) × (fraction of radioactivity representing intact drug) ÷ (specific activity in μCi/mg drug) ÷ (M_r in g/mol). In all cases, the tissue density was assumed to be 1.0 g/cm^3.

DATA ANALYSIS

***In Vitro* Release Kinetics.** The measured drug release from the polymer discs into well-stirred PBS was compared to a model for the diffusional release from a semi-infinite monolithic slab (20):

$$\frac{M_t}{M_\infty} = 4\sqrt{\frac{D_{eff}t}{\pi L^2}} \qquad \text{for } 0 \le \frac{M_t}{M_\infty} \le 0.6 \tag{A}$$

where M_∞ is the initial mass of drug in the polymer, M_t is the cumulative mass of drug released at time t, L is the half-thickness of the polymer disc, and D_{eff} is the effective diffusion coefficient for drug in the polymer matrix.

Local Concentration Profiles. The brain tissue can be modeled as a medium containing three phases: ECS, ICS, and CM (21). In general, the fate of a drug delivered to the brain depends on rates of transport (via diffusion and fluid convection), elimination (by degradation, metabolism, and permeation through blood capillaries), and local binding or internalization. The derivation of the general transport equation, which was described previously (14), is given as follows:

$$\frac{\partial C}{\partial t} = -\nabla\cdot(-\alpha\cdot D_{ECS}\nabla C^0_{ECS} + \alpha\cdot\bar{v}\cdot C^0_{ECS}) - (\alpha\cdot K_{ECS}\cdot C^0_{ECS} + \beta\cdot k_{ICS}\cdot C^0_{ICS} + (1-\alpha-\beta)\cdot K_M\cdot C^0_{CM}) - \frac{\partial B}{\partial t} \tag{B}$$

where C and B represent the number of mol of free and bound chemotherapeutic agent per total brain volume; C^0_{ECS}, C^0_{ICS}, and C^0_{CM} are the mol of drug per phase volume; t is the time following polymer implantation; α and β are the volume fractions of ECS and ICS; D_{ECS} is the diffusion coefficient of the drug in ECS; $\bar{v}$ is the apparent velocity of interstitial fluid in the ECS; and k_{ECS}, k_{ICS}, and k_M are the first-order elimination constants in ECS, ICS, and CM. Assuming steady state and negligible convection, Eq. B, in rectangular coordinates, can be simplified as:

$$D\cdot\frac{\partial^2 C}{\partial x^2} - k\cdot C = 0 \tag{C}$$

where x is the distance from the polymer/tissue interface, D is the apparent diffusion coefficient of the drug in the brain, and k is the apparent first-order elimination constant (see "Appendix A" for details). At steady state, the drug concentration at the polymer/tissue interface (C_i) is constant:

$$C = C_i \qquad \text{for } t > 0; \quad x = 0 \tag{D}$$

Empirically, in concentration profiles obtained from autoradiographic analysis, we observed that the slope of the tangent at the edge of the brain was always 0. Thus, we assumed that the flux at the edge is 0:

$$\frac{\partial C}{\partial x} = 0 \qquad \text{for } t > 0; \quad x = a \tag{E}$$

Applying the two boundary conditions to Eq. C, the steady-state solution is as follows:

$$\frac{C}{C_i} = \frac{\exp\left(-\frac{(a-x)}{L}\phi\right) + \exp\left(\frac{(a-x)}{L}\phi\right)}{\exp\left(-\frac{a}{L}\phi\right) + \exp\left(\frac{a}{L}\phi\right)} \tag{F}$$

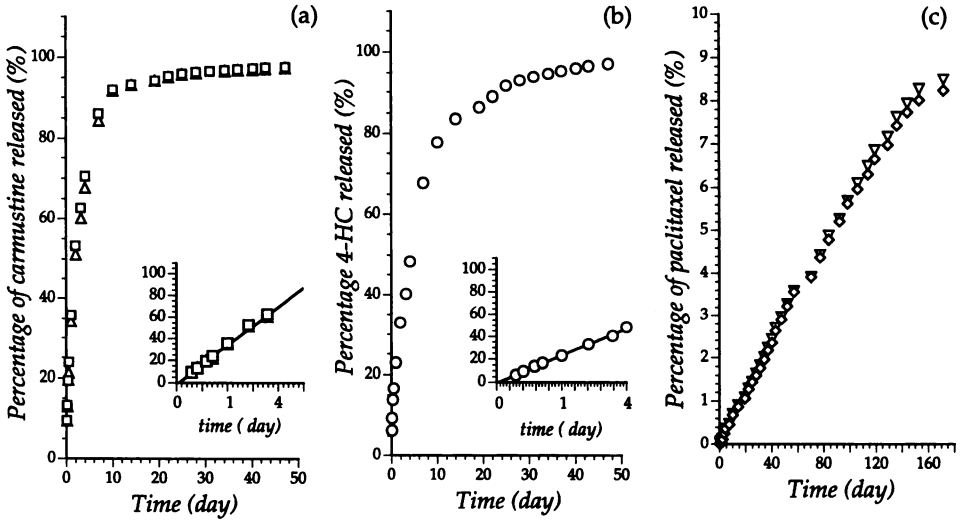

Fig. 3. Release of carmustine in PBS. Each *symbol* represents the cumulative amount of drug released from a carmustine-impregnated (*a*), 4-HC-impregnated (*b*), or paclitaxel-impregnated (*c*) polymer disc. The cumulative mass released was plotted *versus* time (for all three agents) and the square root of time (for carmustine and 4-HC only; *insets* of panels *a* and *b*). The slopes of the solid lines in the insets were determined by linear regression.

where

$$\phi = L \cdot \sqrt{\frac{k}{D}} \qquad \text{(G)}$$

ϕ is the diffusion/elimination modulus, a measure of the relative rates of elimination and diffusion of drugs in the brain tissue; L is the half-thickness of the polymer disc (0.5 mm); a is the perpendicular distance from the polymer/tissue interface to the edge of the brain. The diffusion/elimination modulus was obtained by minimizing the sum of the square of the differences between the calculated concentrations (Eq. F) and experimentally measured concentrations.

Regional Concentrations. Quantitative autoradiography allowed us to measure mM levels of radiolabeled anticancer agents in the region near the polymer discs (*i.e.,* the high-dose region). However, at positions greater than a few mm from the polymer/tissue interface, the local concentration of drug fell below the sensitivity limit of the film. Thus, to measure drug concentrations at locations farther from the polymer disc in the brain, a more sensitive but less precise method was used: drug extraction from coronal sections was followed by TLC and scintillation counting (see "Materials and Methods"). Regional concentrations were calculated based on the total drug mass in each coronal section. Due to the presence of steep concentration gradients within a large volume of tissue, the regional concentration within a 60-μm coronal section (usually in a μM to nM range) is substantially lower than local concentrations measured by autoradiography (usually in a mM range). For example, in a 5-cm^2 coronal section with a typical carmustine concentration gradient at day 7 (C_i, ~0.52 mM; Fig. 5; Table 7), the estimated regional concentration is 5 μM (see Appendix B for details).

Each coronal section is composed of the brain parenchyma, brain vasculature, and ventricular system. The concentration of drug in the brain parenchyma, $\chi_{parenchyma}$, can be calculated by material balance, as follows:

$$\chi_{total} = f_{parenchyma} \cdot \chi_{parenchyma} + f_{blood} \cdot \chi_{blood} + f_{CSF} \cdot \chi_{CSF} \qquad \text{(H)}$$

where χ_{total}, χ_{blood}, and χ_{CSF} are the concentrations or radioactivities in the entire coronal section, blood, and CSF, respectively; $f_{parenchyma}$ (0.888), f_{blood} (0.0226), and f_{CSF} (0.0892) are the volume fractions of the brain parenchyma, blood, and CSF (22), respectively. Rearranging Eq. H yields the following:

$$\chi_{parenchyma} = \frac{\chi_{total} - f_{blood} \cdot \chi_{blood} - f_{CSF} \cdot \chi_{CSF}}{f_{parenchyma}} \qquad \text{(I)}$$

By using Eq. I to calculate the concentrations in the brain parenchyma, we assume that the volume fractions of the parenchyma, vasculature, and ventricular system are the same for all coronal sections.

RESULTS

***In Vitro* Controlled Release.** [^{3}H]Carmustine, [^{3}H]4-HC, and [^{3}H]paclitaxel were continuously released from the 20%-loaded PCPP-SA polymer discs during immersion in PBS (Fig. 3). During the first 4 days of incubation, the release for carmustine and 4-HC was linear with respect to the square root of time (Fig. 3), suggesting that diffusion through the polymer matrix controlled the rate of release. About 70% of the encapsulated carmustine and ~50% of the encapsulated 4-HC were released during the initial 4-day period. In a previous study, degradation and erosion of similar PCPP-SA discs were found to be minimal during the first 4 days of incubation (23); therefore, Eq. A, which assumes no change in polymer matrix structure, appears to be valid in our situation. The effective diffusion coefficients for transport through polymer (D_{eff}) were estimated by comparing Eq. A to the data in Fig. 3, *a* and *b;* the D_{eff} for carmustine was 6.7×10^{-10} cm^2/s, and that for 4-HC was 3.1×10^{-10} cm^2/s. For paclitaxel, ~9% of the encapsulated drug was released at a uniform rate during the first 180 days of incubation; Eq. A was not valid in this case, presumably because the rate of dissolution of paclitaxel into the buffered saline was slower than diffusion through the polymer matrix.

The rate of drug release into PBS can be approximated as follows:

$$\left[\frac{dM_t}{dt}\right]_{saline} = \frac{M_n - M_{n-1}}{t_n - t_{n-1}} \qquad \text{(J)}$$

where t_n is the elapsed time until collection of the nth sample, and M_n is the mass of drug released into the PBS between the fluid exchanges at t_{n-1} and t_n (Fig. 4). During the first 4 days of incubation, carmustine and 4-HC release rates were similar and were higher than the paclitaxel release rate. The rates of release for both carmustine and 4-HC dropped exponentially over time (from ~2 mg/day initially to 1–10 μg/day after 30 days), whereas the rate of release for paclitaxel remained constant over the 30-day period (~3 μg/day).

Tritium Activity in the Blood and CSF. The tritium activity in the blood of animals with carmustine polymer discs implanted were 86% dose/kg fluid (35 pCi/mg) at day 1, 12% dose/kg (~6 pCi/mg) at day 7, and 57% dose/kg (23 pCi/mg) at days 10–30 (Table 1). Tritium activity in the CSF varied in a similar pattern (Table 1).

The tritium activity in both the blood and CSF of animals implanted with 4-HC polymer discs were similar over the 7-day experimental period, ranging from 1.9 to 3.1% dose/kg (0.6–0.9 pCi/mg). All

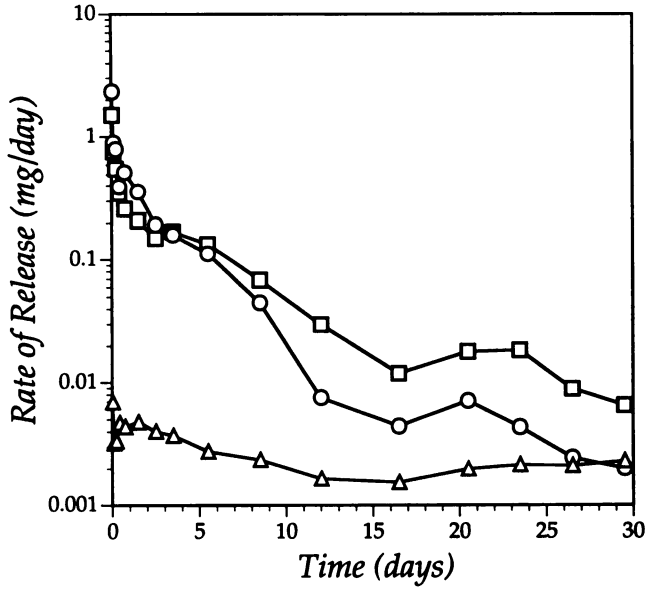

Fig. 4. The rates of release of carmustine (○), 4-HC (□), and paclitaxel (△) from PCPP-SA implants in PBS.

radioactivities were significantly lower than those observed in the carmustine-treated group, although similar amounts of ^3H were given to each animal.

The tritium activity in the blood of animals implanted with paclitaxel polymer discs was even lower: from 0.5% dose/kg (0.2 pCi/mg) at day 1 to 0.1% dose/kg (0.05 pCi/mg) at day 7. No measurable amounts of tritium were observed in the CSF, suggesting that paclitaxel concentrations in CSF were <0.09% dose/kg (0.03 pCi/mg), the limit of detection by scintillation counting.

Carmustine Concentrations in the Blood and CSF. The concentration of chemically intact carmustine in the blood and CSF followed the same trend as the corresponding total tritium activities (Table 2).

Pharmacological Studies. In brain tissue samples obtained 1–5 days after implantation, approximately 10% of the radioactivity in the ipsilateral hemisphere was associated with intact carmustine (Table 3); the percentage was ~3% for samples obtained at days 7–30. The percentage of radioactivity representing intact carmustine in coronal sections closest to the polymer pellet was similar to the average value for the ipsilateral hemispheres (Table 3). In samples from the contralateral hemispheres, the average percentage of extractable, intact carmustine varied between ~1 and ~10%. In animals receiving 4-HC-loaded polymers, the average percentage of extractable, intact 4-HC ranged between 8.4 and 11.6% in the ipsilateral hemisphere and between 1.7 and 11.1% in the contralateral hemisphere (Table 3); in animals receiving paclitaxel-loaded polymers, the average percentage of extractable, intact paclitaxel was between 8.1 and 8.6% in the ipsilateral hemisphere and between 5.7 and 7.9% in the contralateral hemisphere (Table 3).

Regional Concentrations in Coronal Sections. Radioactivity measurements were made in individual coronal brain sections; these levels were converted to average regional concentrations by assuming that the percentage of intact, active drug in each section was equal to the most representative value reported in Table 3. One day after polymer implantation, significant levels of carmustine, 4-HC, and paclitaxel (*i.e.*, μM) were measured at widely distributed locations in all hemispheres of all animals, except for the contralateral hemisphere of the animals given paclitaxel (Tables 4–6). In general, drug concentration at any specific location in the brain decreased with time.

At day 7, in the ipsilateral hemisphere, carmustine concentrations decreased to sub-μM levels ~2 cm from the frontal tip of the brain (Table 4); at the same time, in the contralateral hemisphere, carmustine was not detectable. In the region located 1 and 2 cm from the polymer implant, significant levels of carmustine (0.1–7.5 μM) were measured up to 30 days after polymer implantation. For 4-HC and paclitaxel, significant levels (1–7 μM ipsilaterally and 1–14 μM contralaterally for 4-HC and 0.2–4.8 ipsilaterally for paclitaxel) were measured throughout the 7-day experimental period (Tables 5 and 6).

To estimate the drug concentrations within the brain parenchyma ($\chi_{parenchyma}$), concentrations measured in the blood, CSF, and coronal brain sections were substituted into Eq. I (Tables 4–6). For carmustine, at day 1, μM levels of the drug were measured throughout the entire brain. From days 7 to 30, the extent of distribution (defined as the distance between the frontal tip of the brain and the most posterior coronal section with detectable drug along the anteroposterior axis) of carmustine in the ipsilateral hemisphere decreased from ~3 to ~1.4 cm; within the same time period, no carmustine was measured in the contralateral hemisphere. In the case of 4-HC, tritium activity was detected throughout both hemispheres on days 1 and 3. For paclitaxel, from days 1 to 7, tritium activity was present in the brain parenchyma of the ipsilateral hemisphere but not the contralateral hemisphere.

Local Concentrations in the Vicinity of Polymer Discs. Quantitative concentration profiles were obtained in the vicinity of the polymer from digital images of autoradiograms. Peak levels were always found at the polymer/tissue interface [Table 7; Figs. 5–7 (Please note that Figs. 5–7 show "typical" concentration profiles from single scans, whereas Table 7 lists average values for multiple scans on multiple sections.)]. The concentration of drug at this interface (C_i) was significantly higher (by a factor of 80–450) than the highest of the regional concentrations shown in Tables 4–6 (see Appendix B). For carmustine and paclitaxel, C_i was highest at day 1 and decreased gradually with time; in contrast, C_i for 4-HC-treated animals was constant between days 1 and 7.

To quantify the local penetration of the chemotherapeutic agents, a high-dose region distance was defined by the distance (d_H) from the polymer/tissue interface to a position where the concentration had dropped to 10% of the maximum value (*i.e.*, C_i). Carmustine had the largest high-dose region at day 1 (6.1 mm). From days 3 to 30, d_H fluctuated between 1.1 and 3.6 mm. The high-dose region for 4-HC was smaller than carmustine (between 1.3 and 2.0 mm) in the 7-day experimental period; for paclitaxel, d_H was smallest: 1.3 mm at day 1 and ~0.7 mm at days 3 and 7. By comparing experimental concentration profiles with Eq. F, diffusion/elimination moduli (ϕs) were estimated. Except for day 3, ϕs for carmustine ranged between 0.35 and 0.65 throughout the 30-day period. For 4-HC and paclitaxel, ϕs were ~1 and ~1.6, respectively.

DISCUSSION

The goal of this study was to establish a quantitative pharmacokinetic framework for evaluating the potential benefits of intracerebral polymeric chemotherapy. To achieve this goal, we measured temporal changes in drug concentrations in the blood and CSF, and spatial and temporal changes in drug concentrations in the brain. Brain concentrations were measured locally, in the vicinity of the polymer disc (<3 mm), and regionally over coronal sections from the entire brain (~5 cm). Subsequently, we analyzed these experimental measurements by comparison to a mathematical model based on diffusion, elimination, and binding of drug in the brain.

Carmustine is a lipophilic drug ($P_{o:w}$ = 33.9; Ref. 24) with a low molecular weight (M_r 214) and a low degree of stability and ionization at physiological pH (25, 26). When carmustine is delivered to the brain intrathecally, it is eliminated by hydrolytic degradation

Table 1 *Tritium activity in ipsilateral and contralateral hemispheres, blood, and CSF*[a]

Radioactivity measurements were performed by scintillation counting (tissue samples were digested and blood samples were discolored prior to activity measurements; see "Materials and Methods").

Time following implantation (days)	^{3}H activity in ipsilateral hemisphere (% dose/kg)	^{3}H activity in contralateral hemisphere (% dose/kg)	^{3}H activity in blood (% dose/kg)	^{3}H activity in CSF (% dose/kg)	^{3}H activity in CSF ÷ [^{3}H] activity in ipsilateral hemisphere
Carmustine					
1	14 ± 13	13 ± 14	86 ± 100 (n = 9; m = 4)	100 ± 130 (n = 10, m = 4)	7.1
3	16 ± 13	9.8 ± 4.0	14 ± 2.7 (n = 3; m = 3)	17 ± 16 (n = 5, m = 4)	1.1
7	20 ± 34	1.1 ± 1.7	12 ± 0.6 (n = 3; m = 1)	5.6 ± 0.6 (n = 3, m = 3)	0.3
10–14	11 ± 16	1.0 ± 0.5	77 ± 69 (n = 4, m = 2)	130 ± 130 (n = 3, m = 2)	11
21–30	16 ± 25	4.3 ± 5.7	21, 15 (n = 2, m = 1)	11, 8.2 (n = 2, m = 1)	0.6
4-HC					
1	260 ± 150	81 ± 41	2.3 ± 0.3 (n = 9, m = 2)	1.9 ± 0.3 (n = 5, m = 1)	0.01
3	23 ± 29	17 ± 12	3.1 ± 0.5 (n = 12, m = 2)	2.6 ± 0.5 (n = 9, m = 2)	0.1
7	8.3 ± 9.0	14 ± 6.9	NA	2.1 ± 0.3 (n = 5, m = 1)	0.3
Paclitaxel					
1	10.3 ± 9.8	0	0.5 ± 0.2 (n = 12, m = 2)	0 (n = 10, m = 2)	0
3	2.5 ± 3.9	0	0.3 ± 0.2 (n = 15, m = 2)	0 (n = 12, m = 2)	0
7	1.9 ± 1.8	0	0.1 ± 0.01 (n = 3, m = 1)	0 (n = 3, m = 1)	0

[a] Where indicated, data are means ± SD. n, number of measurements; m, number of animals; NA, not available.

intracellularly [degradation half-life in brain homogenates ($t_{1/2,\ degradation}$) = 110 min; Ref. 27] and transcapillary permeation extracellularly [transcapillary half-life ($t_{1/2,\ transcapillary}$) = 48 s; Ref. 28] (14). Using Eqs. G, A1, and A2 in our diffusion/elimination model, with appropriate parameters (Table 8), the diffusion/elimination modulus, ϕ, can be calculated (1.6). This value of ϕ yields a predicted high-dose distance of ~0.7 mm, consistent with previous measurements made by ventriculocisternal perfusion of radiolabeled carmustine (0.5 mm; Ref. 28). But our autoradiographic analysis indicates that polymeric interstitial delivery of carmustine in monkeys resulted in a high-dose distance substantially higher than the predicted value (1.1–6.1 mm; Table 7). This observed difference suggests that diffusion may not be the sole mechanism of drug migration in the brain when carmustine is delivered intracranially via polymers and is consistent with our previous findings in rats (14), in which we hypothesized that both concentration and pressure gradients contribute to drug transport in the brain.

Enhanced interstitial fluid convection, which is caused by an elevated pressure gradient between the brain interstitium and the ventricular (CSF) space, is a consequence of local edema (29–31). After intracerebral hemorrhage, edema is found to be maximal at 1 day and remains relatively constant for 4 days before beginning to resolve (32). In our experiments, several indirect indicators suggest that edema, and concurrent enhanced interstitial fluid convection, is present in the period immediately after polymer implantation. First, significant levels of carmustine were found in the CSF (Tables 1 and 2). This phenomenon was especially pronounced 1 day after polymer implantation, consistent with our previous study in rats (14). Furthermore, in both monkeys and rats, high levels of carmustine in the CSF were accompanied by extended high-dose distances (6.1 mm in monkeys and 4.7 mm in rats), consistent with the hypothesis that convection of interstitial fluid is important in the early period after implantation. From days 3–30, much lower (4- to 20-fold) levels of carmustine were present in the CSF, and much shorter (approximately two to six times shorter) high-dose distances were measured.

Compared to carmustine-treated animals, significantly lower levels of drug were present in the CSF of 4-HC-treated animals; after paclitaxel treatments, no detectable amounts of drug were measured (Table 1). This comparison suggests that convection-enhanced local drug penetration was less important when 4-HC and paclitaxel were

Table 2 *Carmustine concentrations and percentages of radioactivity representing intact carmustine in the blood (C_{blood}) and CSF (C_{CSF})*[a]

The experimental C_{blood} and C_{CSF} were calculated by the following formula:

Concentration in μM = Tritium activity in fluid in % dose/kg × Weight of loaded carmustine in mg × % carmustine ÷ M_r of carmustine in g/mol ÷ 10

Each polymer disc was loaded with 40 mg of carmustine (M_r = 214). Tritium activity was measured by scintillation counting; percentage of intact carmustine was determined by TLC and scintillation counting. The predicted C_{blood} was computed by a pseudo-steady-state mass balance calculation, as follows:

$$C_{blood,pred} = (k_{transcapillary} \cdot f_{parenchyma} \cdot V_{brain} \cdot C_{brain}) \div (k_{excretion} \cdot V_{blood}),$$

where $k_{transcapillary}$ is the transcapillary rate constant for carmustine (0.0144 s^{-1}; Ref. 28), $f_{parenchyma}$ is the volume fraction of brain parenchyma (0.888; see "Data Analysis"), V_{brain} is the volume of the brain parenchyma of a monkey (62.6 ml, based on an average of five monkey brains), C_{brain} is the weight-averaged regional concentration in a monkey brain (see Table 4), $k_{excretion}$ is the clearance rate of carmustine for i.v. drug delivery (9.96 × 10^{-4} s^{-1}; Ref. 46), and V_{blood} is the volume of blood in a monkey (220 ml; Ref. 47).

Time following implantation	Experimental C_{blood}, μM (% carmustine)	Predicted C_{blood}, μM	Experimental C_{CSF}, μM (% carmustine)
6 h–1 day	3.3 ± 1.9 (n = 5; m = 3) (1.4 ± 0.3)	4.4	11 ± 12 (n = 5, m = 3) (3.0 ± 1.9)
3 days	0.23 ± 0.05 (n = 3; m = 3) (11 ± 3)	NA	0.50 ± 0.38 (n = 3, m = 3) (3.0 ± 1.9)
7 days	0.33 and 0.21 (n = 2; m = 2) (28 and 16)	1.1	0.27 and 0.27 (n = 2, m = 2) (16 and 20)
10–14 days	0.58 ± 0.29 (n = 4; m = 2) (8.8 ± 8.3)	0.2	0.38 ± 0.46 (n = 3, m = 2) (0.9 ± 1.1)
21–30 days	5.0 and 0.9 (n = 2, m = 1) (23 and 5.7)	0.2	2.9 and 0.7 (n = 2; m = 1) (21 and 6.6)

[a] Where indicated, data are means ± SD. n = number of measurements; m = number of animals; NA, not available.

delivered via polymers, consistent with the observed lower high-dose regions in 4-HC- and paclitaxel-treated animals (Table 7; Figs. 6 and 7). Using calculations similar to those performed for carmustine, the predicted ϕs for 4-HC and paclitaxel were 1.5 and 0.2, respectively (see Table 8 legend and footnotes for details). These ϕs correspond to predicted high-dose distances, d_H, of 0.8 mm for 4-HC and >5 mm for paclitaxel. Compared to the experimentally measured d_H, the predicted value for 4-HC represents a slight underestimation, and the predicted value for paclitaxel represents a significant overestimation. The observed high-dose distance of paclitaxel (~0.8–1.3 mm, consistent with a previous study; Ref. 6), which was much shorter than expected based on predictions of our diffusion/elimination model, may be attributed to elimination processes more rapid than spontaneous degradation and transcapillary permeation (*e.g.*, elimination by active transport). In addition, our assumptions of equilibrium binding and partitioning into the membrane phase may not be appropriate for this very insoluble compound. The elimination mechanisms for paclitaxel in the brain are still not well understood.

Autoradiographic analysis demonstrated that high levels of carmustine (C_i = 500-3500 μM), 4-HC (C_i = 330–370 μM), and paclitaxel (C_i = 230–980 μM) were present in the vicinity of the polymer implant (~3 mm). Concentrations in the high-dose region compare favorably to models postulating only diffusive drug transport (Figs. 5–7). But significant levels of drug were also present up to ~5 cm from the polymer implant (Tables 4–6). If diffusion was the dominant mechanism of drug transport, it would take weeks for drug molecules to travel 5 cm (Table 9). Given that this global intracerebral penetra-

Table 3 *Percentage of radioactivity (±SD), representing intact carmustine, 4-HC, and paclitaxel in the monkey brain*

Measurements were made by TLC and scintillation counting.

Time following implantation (days)	% intact agent in section near polymer	% intact agent in ipsilateral hemisphere	% intact agent in contralateral hemisphere
Carmustine			
1	10.5	9.4 ± 4.5	10.9[a]
3	10.1	10.1[a]	3.9 ± 0.9
5	4.6	9.1 ± 5.2	11.9[a]
7	4.0	2.8 ± 2.7	0.6 ± 1.4
14	2.0	2.0 ± 0.4	2.7 ± 0.7
30	3.4	3.6 ± 1.9	2.0 ± 1.3
4-HC			
1	10	8.4 ± 2.3	11.1 ± 6.8
3	10.5	11.6 ± 2.3	4.9 ± 3.3
7	11.4	11.4[a]	1.7 ± 0.6
Paclitaxel			
1	10.6	8.1 ± 3.8	10.5 ± 5.9
3	8.6	8.6[a]	5.7 ± 0.3
7	NA[b]	NA[b]	7.9[a]

[a] Only one or two samples were obtained.
[b] NA, not available.

Table 4 *Regional concentrations of carmustine in the monkey brain*[a]

Measurements were made by TLC and scintillation counting. For each entry, the value in the upper row represents the total regional concentration in a coronal section; the value in the lower row represents the drug concentration in the brain parenchyma of the coronal section, calculated by Eq. I.

Distance from frontal tip of the brain (cm)	Regional carmustine concentrations in ipsilateral coronal sections (μM)			
	Day 1[b]	Day 7[c]	Day 14[c]	Day 30[c]
Implant center[d]	350	30	29	19
	390	34	33	21
1.0–1.3	7.7 (3)	5.0 (1)	1.3 (1)	1.2 (1)
	7.5	5.6	1.3	1.2
1.3–1.5	1.9 (2)	1.9 (1)	0.4 (1)	0.3 (1)
	1.0	2.1	0.3	0.2
1.5–2.0	1.7 (3)	0.9 (1)	0.1 (1)	0.06 (1)
	0.8	1.0	0	0
2.0–3.0	1.7 (3)	0.13 (2)	<0.004	NA
	0.8	0.1	ND	NA
3.0–4.0	1.8 (2)	0.05 (2)	<0.004	0.05 (1)
	0.9	0	ND	0
4.0–5.0	1.4 (1)	0.04 (2)	<0.004	0.05 (2)
	0.4	0	ND	0
	Regional carmustine concentrations in contralateral coronal sections (μM)			
0–1.0	4.7 (3)	<0.001	<0.005	0.08 (2)
	4.1	ND	ND	0
1.0–2.0	2.2 (3)	<0.001	<0.005	<0.004
	1.3	ND	ND	ND
2.0–3.0	1.1 (1)	NA	<0.005	0.10 (2)
	0	NA	ND	0
3.0–5.0	1.3 (9)	<0.001	NA	0.07 (4)
	0.3	ND	NA	0

[a] Numbers of samples appear in parentheses; NA, not available for analysis; ND, below detection limits.
[b] Percentage of carmustine estimated from average of three measurements.
[c] Percentage of carmustine measured individually for each sample.
[d] Calculations for total regional concentrations in coronal sections bisecting the midline of the implant were based on autoradiographic analysis (see Table 7; also see Appendix B for sample calculation).

Table 5 *Regional concentrations of 4-HC in the monkey brain*[a]

Measurements were made by TLC and scintillation counting. For each entry, the value in the upper row represents the total regional concentration in a coronal section; the value in the lower row represents the drug concentration in the brain parenchyma of the coronal section, calculated by Eq. I.

Distance from frontal tip of the brain (cm)	Regional 4-HC concentrations in ipsilateral coronal sections (μM)		
	Day 1	Day 3	Day 7
Implant center[b]	6.7	8.0	5.7
	7.5	9.0	NBS
2.0–3.0	7.0 ± 5.0 (7)	3.4 ± 3.2 (10)	1.8 ± 1.7 (4)
	7.8	3.8	NBS
3.0–4.0	5.2 ± 2.7 (9)	0.9 ± 0.6 (5)	0.9 ± 0.8 (3)
	5.8	1.0	NBS
4.0–5.0	2.7 ± 1.3 (4)	1.4 ± 0.9 (11)	0.9 ± 0.6 (3)
	3.0	1.5	NBS
	Regional 4-HC concentrations in contralateral coronal sections (μM)		
0–1.0	13.9 ± 4.2 (6)	13.8 (1)	0.8 (1)
	15.6	15.6	NBS
1.0–2.0	5.1 ± 1.4 (12)	3.8 ± 0.6 (10)	2.1 ± 0.1 (3)
	5.7	4.3	NBS
2.0–3.0	2.4 ± 0.5 (7)	1.8 ± 0.1 (7)	1.9 ± 0.03 (4)
	2.7	2.0	NBS
3.0–4.0	1.9 ± 0.3 (6)	2.4 ± 0.3 (6)	NA
	2.1	2.7	NA
4.0–5.0	2.4 ± 0.1 (5)	3.4 ± 0.5 (4)	NA
	2.7	3.8	NA

[a] Numbers of samples appear in parentheses. Where indicated, data are means ± SD. NA, not available for analysis; NBS, not available due to lack of blood sample.
[b] Calculations for total regional concentrations in coronal sections bisecting the midline of the implant were based on autoradiographic analysis (see Table 7; see also "Appendix B" for sample calculation).

Table 6 *Regional concentrations of paclitaxel in the monkey brain*[a]

Measurements were made by TLC and scintillation counting. No detectable concentrations of paclitaxel were observed in the contralateral coronal sections (detection limit, 0.003 μM). For each entry, the value in the upper row represents the total regional concentration in a coronal section; the value in the lower row represents the drug concentration in the brain parenchyma of the coronal section, calculated by Eq. I.

Distance from frontal tip of the brain (cm)	Regional paclitaxel concentrations in ipsilateral coronal sections (μM)		
	Day 1	Day 3	Day 7
Implant center[b]	10.3	3.4	2.6
	11.6	3.8	2.9
2.0–3.0	2.5 ± 3.6 (4)	1.5 ± 1.65 (5)	0.2 ± 0.1 (3)
	2.8	1.7	0.2
3.0–4.0	4.8 ± 2.6 (5)	0.3 ± 0.2 (4)	0.7 ± 0.6 (3)
	5.4	0.3	0.8
4.0–5.0	0.5 (1)	0.2 ± 0.04 (3)	NA
	0.6	0.2	NA

[a] Numbers of samples appear in parentheses. Where indicated, data are means ± SD. NA, not available for analysis.
[b] Calculations for total regional concentrations in coronal sections bisecting the midline of the implant were based on autoradiographic analysis (see Table 7; see also "Appendix B" for sample calculation).

tion was achieved within 1 day after implantation in animals treated with all three drug compounds, transport mechanisms other than diffusion must be involved. The convection velocity due to edema ranges from 0.2 to 3.4 mm/day (14, 33), so that movement of edema fluid is more rapid than diffusion (Table 9). This faster rate of transport can account for the enhanced local penetration observed in the 1-cm region closest to the polymer 1 day after carmustine treatment (see above). But convection is not fast enough to account for drug migration of 5 cm in 1 day (Table 9).

Two transport mechanisms could account for global drug penetration: (*a*) permeation of drug into the CSF, circulation within the ventricles and subarachnoid space, and subsequent diffusion back into the ECS through an ependymal or pial surface distant from the implant, and (*b*) permeation through the BBB, which may be leaky at the site of corticotomy; circulation in the cerebral vasculature; and reentry back into the brain parenchyma.

The velocity of CSF in the cervical subarachnoid space of the brain is 11–52 mm/s in humans (34); thus, the characteristic time for CSF movement in the brain is ~2 s (Table 9). Because the CSF and interstitial fluid are in close communication via the pial and ependymal surfaces (Fig. 8), the characteristic time for drug exchange is very short (5.7 s; Table 9). Therefore, the transport of drugs by CSF flow and reentry seems to be a plausible mechanism for drug distribution over a long distance in the brain.

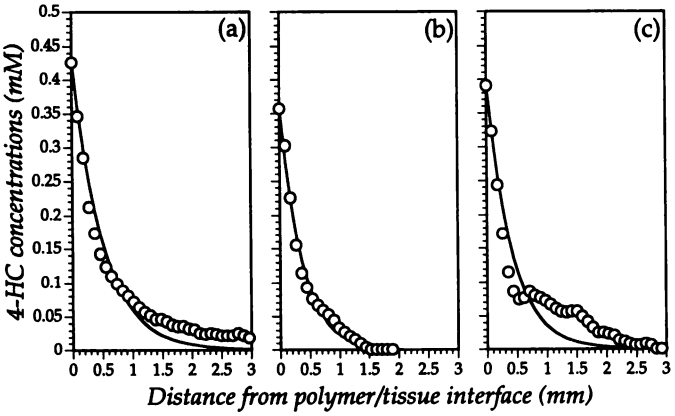

Fig. 6. Concentration profiles of free 4-HC in the vicinity of polymer implants. Positions of the *symbols* were determined by scanning individual coronal sections and determining the concentration as a function of distance from the edge of the polymer at days 1 (*a*), 3 (*b*), and 7 (*c*). ——, steady-state diffusion/elimination model, in which ϕ was varied to compare most favorably with the experimental data.

Table 7 *Summary of concentration profiles of carmustine, 4-HC, and paclitaxel in the monkey brain*[a]

Concentration profiles were obtained by quantitative autoradiography. Drug concentrations were calculated by using the percentage of intact drug for a coronal section closest to the polymer disc, as reported in Table 4. C_i is the drug concentration at the polymer/tissue interface; d_H is the high-dose distance, defined as the distance from the polymer/tissue interface to a position in the brain tissue where concentration is 10% of C_i; ϕ is the diffusion/elimination modulus, determined by adjusting the modulus so that concentrations calculated by Eq. F match experimental concentrations. Data are means ± SD.

Time following implantation (days)	C_i (μM)	d_H (mm)	ϕ
Carmustine			
1	3500 ± 1500	6.1 ± 2.9	NA
3	1700 ± 230	1.1 ± 0.57	1.2 ± 0.53
5	1790 ± 190	3.6 ± 1.3	0.50 ± 0.19
7	520 ± 100	2.6 ± 0.57	0.36 ± 0.08
14	500 ± 100	2.9 ± 0.69	0.35 ± 0.07
30	630 ± 40	1.8 ± 0.97	0.65 ± 0.27
4-HC			
1	350 ± 110	1.7 ± 0.81	1.0 ± 0.33
3	370 ± 70	1.3 ± 0.36	0.90 ± 0.36
7	330 ± 80	2.0 ± 0.63	1.1 ± 0.17
Paclitaxel			
1	980 ± 830	1.3 ± 0.96	1.7 ± 0.33
3	320 ± 100	0.72 ± 0.20	1.7 ± 0.41
7	230 ± 20	0.77 ± 0.14	1.6 ± 0.32

[a] NA, not applicable because steady state was not reached at day 1.

Drug permeation through capillary wall, circulation within the brain vasculature, and reentry back into the brain parenchyma constitute another possible mechanism for drug distribution (Fig. 8). We know that drug molecules, particularly carmustine, enter the systemic circulation; carmustine concentrations predicted by pseudo-steady-state mass balance calculations between the brain and vascular compartments agreed reasonably well with the experimentally measured values (Table 2). According to Renkin (35), one phase of tissue injury response is retraction of endothelial cells in pericytic venules; this creates μm-wide gaps in capillary walls, resembling those of discontinuous or fenestrated endothelium. Fenestrated capillaries can also be found in healthy tissues at the choroid plexus of the brain and the ciliary body of the eye and in the vasculature of certain tumors in the brain and other tissues (36). The permeability of fenestrated capillaries is higher than nonfenestrated or intact capillaries (37, 38); experiments using similar polymer capsules in rats indicate that repair of the fenestrated endothelium takes approximately 50 days after polymer implantation (39). Because the hydraulic conductivity for fenestrated capillaries is very high (35), the characteristic time for leakage

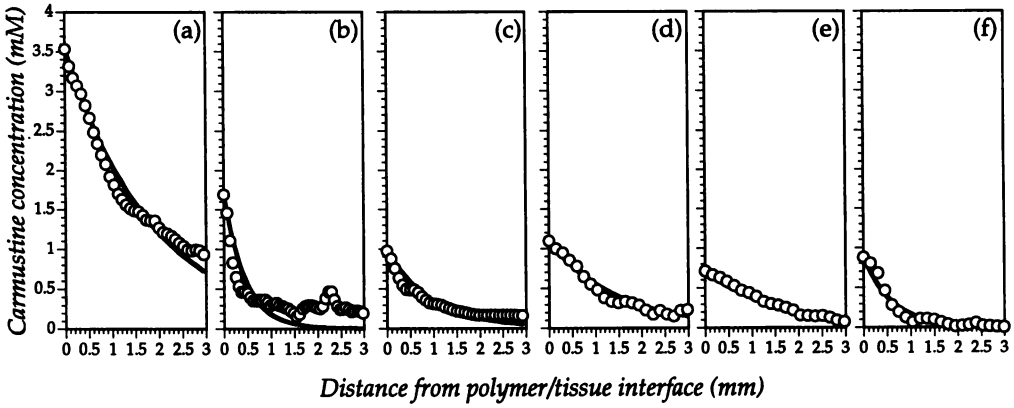

Fig. 5. Concentration profiles of free carmustine in the vicinity of polymer implants. Positions of the *symbols* were determined by scanning individual coronal sections and determining the concentration as a function of distance from the edge of the polymer at days 1 (*a*), 3 (*b*), 5 (*c*), 7 (*d*), 14 (*e*), and 30 (*f*). ——, steady-state diffusion/elimination model, in which ϕ was varied to compare most favorably with the experimental data.

Table 8 *Physicochemical and pharmacological properties for carmustine, 4-HC, and paclitaxel*[a]

$P_{o:w}$ is the octanol-water partition coefficient; D_{ECS} is the drug diffusion coefficient in the brain; $t_{1/2,\ degradation}$ is the drug degradation half-life in the brain; $t_{1/2,\ transcapillary}$ is the extracellular fluid-transcapillary half-life. $\phi_{predicted}$ was calculated by using Eqs. G, A1, and A2, assuming that $k_{ics} = \ln 2/t_{1/2,\ degradation}$, $k_{ecs} = \ln 2/t_{1/2,\ transcapillary}$, and $P_{i:e} = 1$. $\phi_{experimental}$ is the experimental diffusion/elimination modulus (Table 7). LD_{90} is the dose of a chemotherapeutic agent that kills 90% of the testing cell population of cells *in vitro*.

	Carmustine	4-HC	Paclitaxel
Empirical formula	$C_5H_9Cl_2N_3O_2$	$C_7H_{15}Cl_2N_2O_2P$	$C_{47}H_{51}NO_{14}$
Molecular weight	214.0	261.1	853.9
log $P_{o:w}$	1.53 (24)	0.77 (51)	3.5 (52)
D_{ECS} ($\times 10^{-6}$ cm^2/s)	14.3 (28)	12.9[b]	9.0
$t_{1/2,\ degradation}$ (min)	110 (27)	22 (53)	17,000 (Appendix C)
$t_{1/2,\ transcapillary}$ (min)	0.8 (28)	2.9[c]	83[d]
$\phi_{predicted}$	1.6	1.5	0.2
$\phi_{experimental}$	0.4–1.2	0.9–1.1	1.6–1.7
Target	O^6-Guanine in DNA	N^7-Guanine in DNA	NH_2-terminal 31 amino acids of β-tubulin
Plasma or surface proteins to be bound	Albumin (26)	NA	Albumin, α_1-acid-glycoprotein (54)
Cytotoxic metabolites	Chloroethyl-diazonium ion (55)	Phosphoramide, acrolein, nornitrogen mustard (56)	6α-Hydroxytaxol (57, 58)
Noncytotoxic metabolites	2-Chloroethanol, alkylated nucleic acid, and carbamoylated proteins (59)	Aldophosphamide, 4-ketocyclophosphamide, carboxyphosphamide (56)	NA
LD_{90} for 1-h treatment (μM)	15 (U-251 MG human glioma cells; Ref. 60)	12.8 (TE-671 human medulloblastoma cells; Ref. 51)	0.89 (9L rat glioma cells; Ref. 61)

[a] NA, not available. Reference numbers appear in parentheses.

[b] Calculations for 4-HC and paclitaxel were based on the Stokes-Einstein relationship.

[c] Calculations for 4-HC were based on correlations in Ref. 48 and a brain capillary surface area of 240 cm^2/g (49).

[d] Calculations for paclitaxel used a mass balance equation: $t_{1/2,\ transcapillary} = \ln 2/k_{ECS} = (V_{brain}\ C_{brain}\ t_{1/2,\ excretion}) \div (V_{blood}\ C_{blood})$, where V_{brain} is the volume of brain parenchyma for a monkey (62.6 × 0.888 = 55.6 ml; 62.6 ml is the total volume of a monkey brain, averaged over five monkeys; 0.888 is the fraction of brain parenchyma in a monkey brain; Ref. 22); C_{brain}, calculated from values in Table 6, is the average concentration of paclitaxel in the brain; $t_{1/2,\ excretion}$ is the β clearance half-life of i.v. paclitaxel, administered for 5.8 h (50); V_{blood} is the plasma volume for a monkey, 220 ml (47); and C_{blood} is the concentration of paclitaxel in the blood (see Table 1).

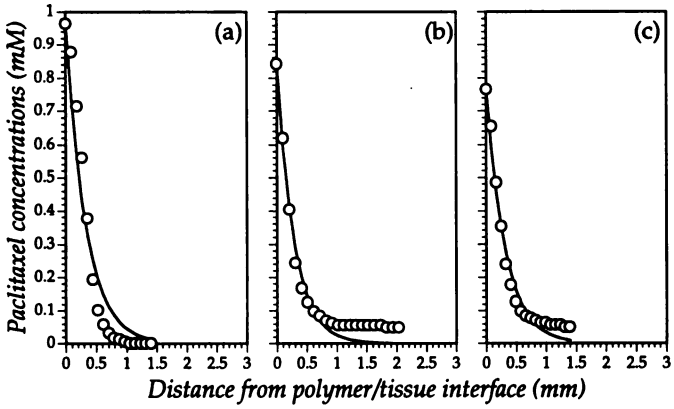

Fig. 7. Concentration profiles of free paclitaxel in the vicinity of polymer implants. Positions of the *symbols* were determined by scanning individual coronal sections and determining the concentration as a function of distance from the edge of the polymer at days 1 (*a*), 3 (*b*), and 7 (*c*). ——, steady-state diffusion/elimination model, in which ϕ was varied to compare most favorably with the experimental data.

of drugs from interstitium into cerebral capillaries in the vicinity of the implant should be very short (0.5 s; Table 9). On the basis of the blood flow rate in cerebral capillaries, the characteristic time for cerebral blood flow was calculated to be 10 s (Table 9). Thus, minimal drug degradation should occur in the period when drug molecules travel with the cerebral blood to distant sites from the polymer implant. The reentry of drug molecules into the brain interstitium at sites distant from the polymer (via intact endothelium) therefore depends on the permeability of the BBB to the drug (Table 9).

In summary, drug distribution by diffusion through the interstitium (enhanced by induced convection in the case of carmustine) can account for drug distribution in the high-dose region near the polymer. Drug movement facilitated by both cerebral blood and CSF flows appears to be important for drug transport to distant locations in the brain. Our experimental data are consistent with this hypothesis. Carmustine and 4-HC were present at distant locations from the

Table 9 *Characteristic times for transport of drug released by polymeric pellets in the brain*

The characteristic length scale, L_{brain} (5 cm), was chosen to be the maximum distance with measurable amounts of drug along the anteroposterior axis. D_{ECS}, diffusion coefficient of drug in extracellular space [14×10^{-6} cm^2/s for carmustine (28); 13×10^{-6} cm^2/s for 4-HC; 9×10^{-6} cm^2/s for paclitaxel; values for 4-HC and paclitaxel are based on the Stokes-Einstein relationship); $d_{capillary}$, thickness of endothelial wall (0.1 μm; Ref. 62)]; ΔP, difference between capillary and interstitial hydrostatic pressures (~1 mm Hg; Ref. 36); L_p, hydraulic conductivity (15×10^{-9} and 3.0×10^{-13} cm^3/s-dyne for fenestrated capillaries and tight junction, respectively; Ref. 38); f_{blood}, volume fraction of vasculature in the monkey brain (0.0226; Ref. 22); v_{blood}, blood velocity in cerebral capillaries (5 mm/s; Ref. 63); $k_{transcapillary}$, transcapillary elimination constant [0.014 s^{-1} for carmustine (28); 1.53×10^{-5} s^{-1} for 4-HC, based on correlations in Ref. 48]; $d_{ependyma}$, size of an ependymal cell (1 μm); $v_{ISF\text{-}CSF}$, velocity for ISF toward the ventricle (10.5 μm/min; Ref. 64); f_{CSF}, volume fraction of ventricular system in the monkey brain (0.0892; Ref. 22); v_{CSF}, CSF velocity in cervical subarachnoid space (~30 mm/s; Ref. 34).

	Transport process(es)[a]	Equations for characteristic times	Characteristic times
(i)	Diffusion	L^2_{brain}/D_{ECS}	20 days (carmustine) 22 days (4-HC) 32 days (paclitaxel)
(ii)	Convection	L_{brain}/v_{ISF}	15 days (carmustine in normal brain; Ref. 14) 8 days (induced vasogenic edema; Ref. 33)
(iii) a	Drug permeation	$d_{ependyma}/v_{ISF\text{-}CSF}$	5.7 s
		$d^2_{ependyma}/D_{ECS}$	~0 s
b	CSF flow	L_{brain}/v_{CSF}	1.7 s
(iv) a	Drug leakage	$d_{capillary}/L_p\Delta P$	0.5 s (fenestrated capillary) 7 h (tight junction)
b	Blood flow	L_{brain}/v_{blood}	10 s
c	Drug reentry	$d_{capillary}/L_p\Delta P$	0.5 s (fenestrated capillary)
		$\ln 2/k_{transcapillary}$	0.8 min (carmustine, tight junction) 2.9 min (4-HC, tight junction) 83 min (paclitaxel, tight junction)

[a] See legend to Fig. 8 for an explanation of transport processes i–iv.

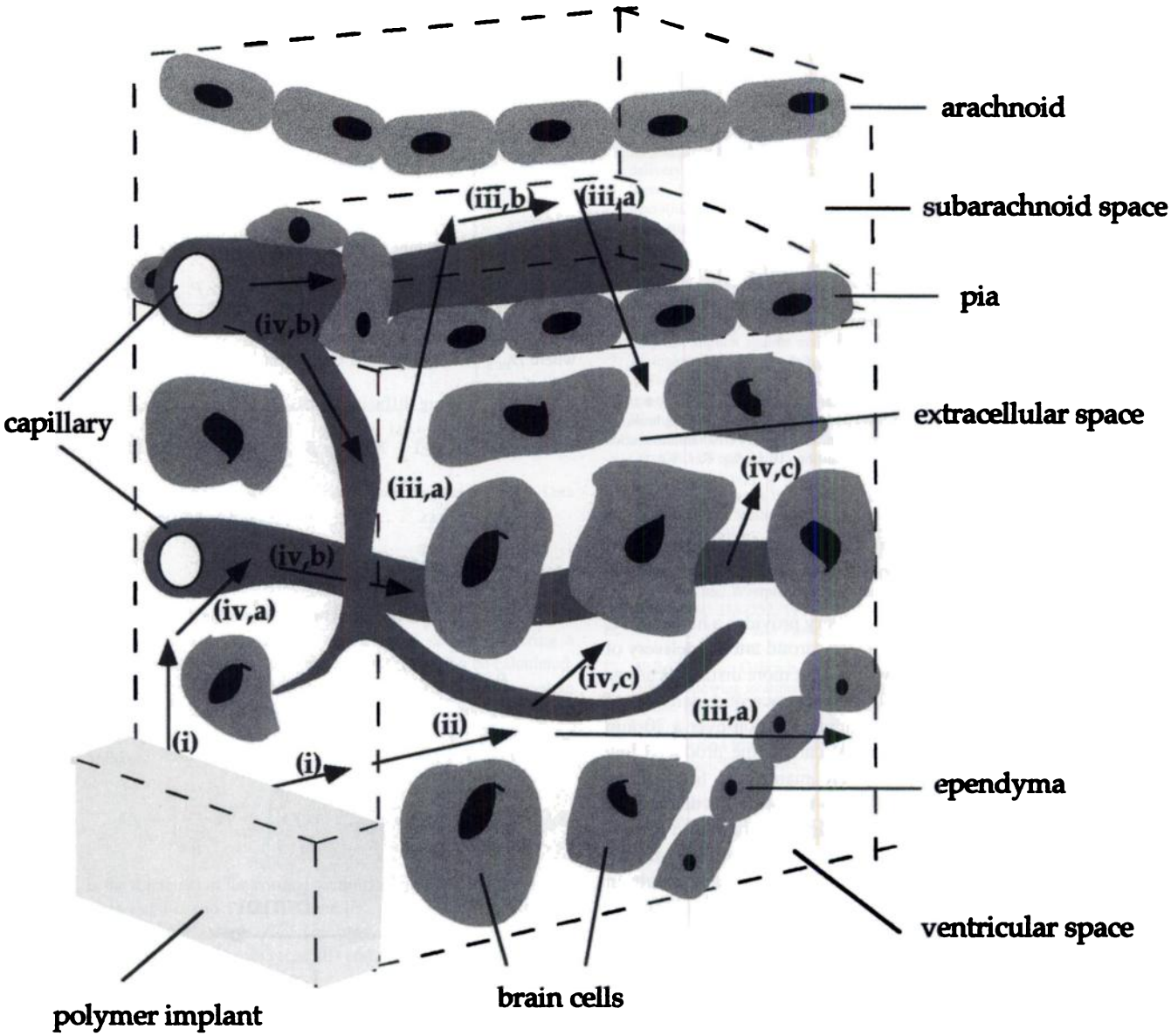

Fig. 8. Fate of drug released from the polymer pellet to the brain. After drug molecules are released from the polymer matrix, they enter the ECS of the brain; they can be transported by diffusion due to drug concentration gradients (*i*); convection due to fluid pressure gradients (*ii*); drug migration into ventricular space via pial or ependymal surfaces (*iii,a*), circulation in the subarachnoid or ventricular spaces (*iii,b*), and subsequent diffusion back into the brain interstitium (*iii,c*); and permeation through the endothelium (*iv,a*), circulation in the cerebral blood vessels (*iv,b*), and reentry by permeation back into the brain interstitium (*iv,c*).

polymer disc in both the ipsilateral and contralateral hemispheres in concentrations that correlated with levels in the blood and CSF (Table 1). On the contrary, paclitaxel was not found in the CSF and contralateral hemisphere, and only low concentrations were found in blood and distant ipsilateral tissue. The extent of drug reentry at distant sites should be greatest for molecules with the highest permeability in intact BBB (Table 9); the experimental data follow the expected trend, with more extended distribution in carmustine- and 4-HC-treated animals than in paclitaxel-treated animals.

Potential Benefits of Polymeric Chemotherapy in Brain Tumor Treatment. Concentrations in the vicinity of the polymer discs (Table 7; Figs. 5–7) were very high, compared with cytotoxic concentrations of these agents *in vitro* (see LD_{90} values in Table 8). In the first 7 days after implantation, the ratio of concentration at the polymer/tissue interface and LD_{90} ($C_{i,brain}$:LD_{90}) ranged from 110 to 230 for carmustine, from 26 to 29 for 4-HC, and from 260 to 1100 for paclitaxel. The actual cytotoxic potential should exceed the calculated $C_{i,brain}$:LD_{90} ratio, because the period of drug exposure following polymer implantation (1–30 days) was much longer than the *in vitro* treatment period used to determine LD_{90} (1 h). To account for the temporal drug exposure to the brain, the AUC was calculated by considering regional drug concentrations measured at different times and positions in the brain (Fig. 9). Because <1% of paclitaxel was released from polymers in a 7-day incubation period (Fig. 3), the AUC for longer-term treatment of paclitaxel should be much higher (6). In tissue in the vicinity of the polymer disc (~1 cm), a 30-day delivery of carmustine produced an AUC two times greater than the AUC for a 7-day treatment. This effect was less pronounced at more distant locations from the polymer in the brain. More importantly, both 7- and 30-day polymeric treatments (~8 mg/kg) provided a higher AUC than i.v. delivery of a higher dose (10 mg/kg) (40). To obtain the same AUC achieved by polymeric delivery at distant locations from the pellet (100–200 μM-h), the required i.v. dose must be at least four times higher (>40 mg/kg); to obtain the AUC in the vicinity of the

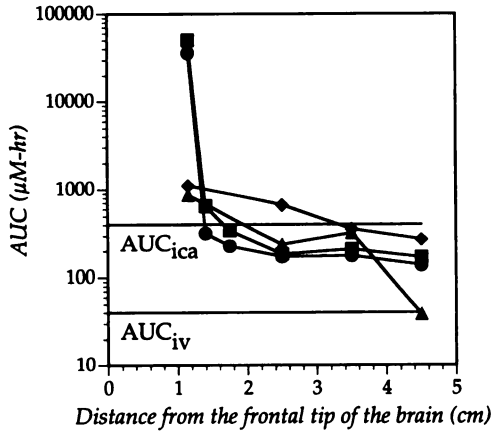

Fig. 9. The AUC for carmustine [7-day (●) and 30-day (■) exposures], 4-HC (◆), and paclitaxel (▲) delivered by intracerebrally implanted polymers (8 mg/kg) to the brain, as compared to the AUC for carmustine delivered by intracarotid artery (*ica*) administration with hemoperfusion (10 mg/kg) and i.v. (*iv*) administration (10 mg/kg; Ref. 40).

polymer (1,000–50,000 μM-h), i.v. treatment would require a dose of 250–12,500 mg/kg. These doses would certainly lead to intolerable side effects (41).

The 30-day treatment of polymeric delivery provides a higher AUC in the vicinity of the polymer disc than intracarotid arterial delivery of carmustine (40), but it provides a lower AUC at more distant locations in the brain (Fig. 9). The high AUC for intracarotid delivery of carmustine was achieved by high-dose administration over a 20-min period. In contrast, polymeric delivery of carmustine produced low concentrations of carmustine, which were maintained for a much longer period. Human clinical trials using intra-arterial delivery of carmustine demonstrated reduced survival in patients due to serious systemic toxicity (42). In contrast, intracerebral delivery of carmustine by 20% drug-loaded polymer pellets did not result in systemic side effects, such as leukopenia and thrombocytopenia (43). Recently, we demonstrated that low concentrations of carmustine delivered by polymers to glioma cell cultures were as effective in reducing cell proliferation as carmustine delivered by a bolus addition at the same dose (44). Thus, polymeric chemotherapy, which provides a low-concentration, long-term delivery of anticancer agents to a large volume of the brain is potentially more effective and less toxic than traditional short-term, high-concentration delivery techniques.

In summary, we performed a detailed study on the distribution of carmustine, 4-HC, and paclitaxel delivered by an implanted, biodegradable polymer matrix in the primate brain. This study presents the first experimental evidence that extremely high concentrations of intact drug (mM levels) are achieved in the vicinity of the implantation site and that low concentrations (μM levels) are maintained at distant locations in the brain for a prolonged period after a single dose of polymer-encapsulated drug. Although high drug concentrations maintained near the polymer pellet can prevent local tumor recurrence, the prolonged, low-concentration exposure of chemotherapy suggests that this delivery modality may be effective in treating multifocal gliomas and tumors that recur at sites distant from the primary tumor.

ACKNOWLEDGMENTS

We thank Dr. Abraham Domb for making some of the polymer pellets; Dr. Susan Ludeman and Carol Hartke for synthesizing [^{3}H]4-HC; Susan Roberts for running paclitaxel samples by high-performance liquid chromatography; Dr. John Hilton, Dr. Mollie Wagster, and Joyce Kotcuk for helpful discussions; and Betty Tyler, Michael Pinn, Kate Shannon, Kara Shaffer, Akiko Omura, Mark Travis, Joseph Ismert, and Patrick Schloss for technical assistance.

APPENDIX A

Apparent diffusion coefficient (D):

$$D = \frac{\alpha}{\alpha^*} D_{ECS} \tag{A1}$$

Apparent elimination constant (k):

$$k = \frac{\alpha \cdot k_{ECS} + \beta \cdot k_{ICS} \cdot P_{i:e}}{\alpha^*} \tag{A2}$$

where D_{ECS} = drug diffusion coefficient in the ECS

D_{ECS} = drug diffusion coefficient in the extracellular space

$$\alpha^* = \alpha \cdot (1 + K_{ECS}) + \beta \cdot P_{i:e} \cdot (1 + K_{ICS}) + (1 - \alpha - \beta) \cdot P_{m:e} \tag{A3}$$

$$K_{ECS} = \frac{B^0_{ECS}}{C^0_{ECS}} \tag{A4}$$

$$K_{ICS} = \frac{B^0_{ICS}}{C^0_{ICS}} \tag{A5}$$

$$P_{i:e} = \frac{C^0_{ICS}}{C^0_{ECS}} \tag{A6}$$

$$P_{m:e} = \frac{C^0_{CM}}{C^0_{ECS}} \tag{A7}$$

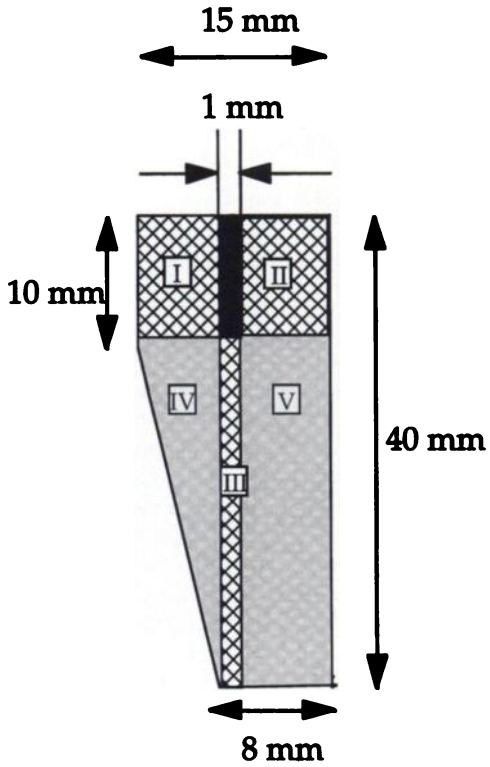

Appendix Fig. 1. A schematic representation of a coronal monkey brain section bisecting a polymer pellet (*black rectangle*). Drug mass in the *hatched areas* (I, II, III) is significantly higher than in the *gray areas* (IV, V).

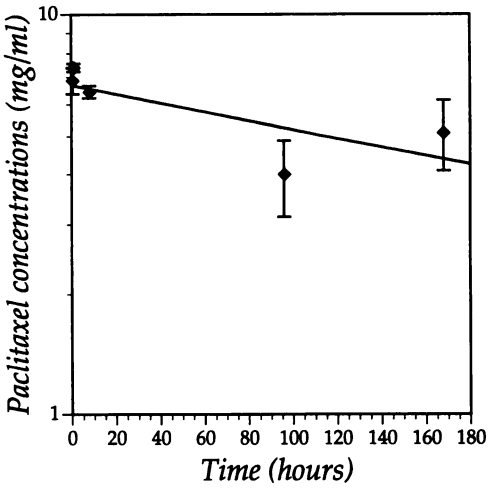

Appendix Fig. 2. Concentrations of paclitaxel in rat brain homogenates at 37°C. Data are means; *bars,* SD.

APPENDIX B

Sample Calculation of Regional Concentrations from Local Concentrations. Using an approximate geometry for the coronal section bisecting a polymer pellet (Appendix Fig. 1), the regional concentration can be calculated. The coronal section can be divided into five zones: zones I–III contain significantly higher drug mass than do zones IV and V. To compute the amount of drug in zones I–III (M_n), the concentration profiles in these regions can be integrated as follows:

$$M_n = \int_n C \cdot dV = \int_n C(x) \cdot t_{section} \cdot w_n \cdot dx \qquad (A8)$$

where $t_{section}$ is the thickness of the coronal section, w_n is the width of the zone (10 mm for zones I and II and 1 mm for zone III), and x is the perpendicular distance from the polymer surface. $C(x)$ can be evaluated using Eq. F, with a = 7 mm (zones I and II) or 30 mm (zone III) and L = 0.5 mm. The regional concentration can be computed as follows:

$$\text{Regional concentration} = \frac{\sum_{I-III} M_n}{t_{section} \cdot A_{section}} \qquad (A9)$$

where $A_{section}$ is the area of the coronal section, 495 mm^2.

Consider a local concentration gradient for carmustine at day 7: C_i = 0.52 mM; ϕ = 0.36. Using Eqs. F, A8, and A9, the regional concentration is 30 μM, which agrees reasonably well with the experimentally measured concentration in a region near the center of the polymer implant (5 μM; Table 4).

APPENDIX C

Paclitaxel Degradation Study. Paclitaxel (50 μl; 70 mg/ml in ethanol) was added to rat brain homogenates (rat brain tissue sonicated with PBS in a 1:3 ratio; 450 μl), and kept at 37°C under gentle agitation. Periodically, the mixture was extracted with methylene chloride (500 μl) three times. The extracts were pooled and then evaporated to dryness, and the residue was resuspended in methanol (500 μl) and filtered through a 0.22-μm filter. The filtrates were analyzed by reverse-phase high-performance liquid chromatography with photodiode array detection, as described previously (45). Assuming first-order degradation of paclitaxel, the half-life of paclitaxel in brain homogenates was ~280 h (Appendix Fig. 2).

REFERENCES

1. Brem, H., Mahaley, S. M., Jr., Vick, N. A., Black, K. L., Schold, S. C., Jr., Burger, P. C., Friedman, A. H., Ciric, I. S., Eller, T. W., Cozzens, J. W., and Keneally, J. N. Interstitial chemotherapy with drug polymer implants for the treatment of recurrent gliomas. J. Neurosurg., *74:* 441–446, 1991.
2. Brem, H., Piantadosi, S., Burger, P. C., Walker, M., Selker, R., Vick, N. A., Black, K., Sisti, M., Brem, S., Mohr, G., Muller, P., Morawetz, R., and Schold, S. C. Placebo-controlled trial of safety and efficacy of intraoperative controlled delivery by biodegradable polymers of chemotherapy for recurrent gliomas. Lancet, *345:* 1008–1012, 1995.
3. Tamargo, R. J., Myseros, J. S., Epstein, J. I., Yang, M. B., Chasin, M., and Brem, H. Interstitial chemotherapy of the 9L gliosarcoma: controlled release polymers for drug delivery in the brain. Cancer Res., *53:* 329–333, 1993.
4. Sipos, E. P., Tyler, B., Piantadosi, S., Burger, P. C., and Brem, H. Optimizing interstitial delivery of BCNU from controlled release polymers for the treatment of brain tumors. Cancer Chemother. Pharmacol., *39:* 383–389, 1997.
5. Judy, K. D., Olivi, A., Buahin, K. G., Domb, A., Epstein, J. I., Colvin, O. M., and Brem, H. Effectiveness of controlled release of a cyclophosphamide derivative with polymers against rat gliomas. J. Neurosurg., *82:* 481–486, 1995.
6. Walter, K. A., Cahan, M. A., Gur, A., Tyler, B., Hilton, J., Colvin, O. M., Burger, P. C., Domb, A., and Brem, H. Interstitial Taxol delivery from a biodegradable polymer implant against malignant glioma. Cancer Res., *54:* 2207–2212, 1994.
7. Weingart, J. D., Thompson, R. C., Tyler, B., Colvin, O. M., and Brem, H. Local delivery of the topoisomerase I inhibitor camptothecin sodium prolongs survival in the rat intracranial 9L gliosarcoma model. Int. J. Cancer, *62:* 605–609, 1995.
8. Weingart, J. D., Sipos, E. P., and Brem, H. The role of minocycline in the treatment of intracranial 9L glioma. J. Neurosurg., *82:* 635–640, 1995.
9. Olivi, A., Ewend, M. G., Utsuki, T., Tyler, B., Domb, A. J., Brat, D. J., and Brem, H. Interstitial delivery of carboplatin via biodegradable polymers is effective against experimental glioma in the rat. Cancer Chemother. Pharmacol., *39:* 90–96, 1996.
10. Ewend, M. G., Williams, J. A., Tabassi, K., Tyler, B. M., Babel, K. M., Anderson, R. C., Pinn, M. L., Brat, D. J., and Brem, H. Local delivery of chemotherapy and concurrent external beam radiotherapy prolongs survival in metastatic brain tumor models. Cancer Res., *56:* 5217–5223, 1996.
11. Giese, A., and Westphal, M. Glioma invasion in the central nervous system. Neurosurgery, *39:* 235–252, 1996.
12. Hochberg, F. H., and Pruitt, A. Assumptions in the radiotherapy of glioblastoma. Neurology, *30:* 907–911, 1980.
13. Wallner, K. E., Galicich, J. H., Krol, G., Arbit, E., and Malkin, M. G. Patterns of failure following treatment of glioblastoma multiforme and anaplastic astrocytoma. J. Radiat. Oncol. Biol. Phys., *16:* 1405–1409, 1989.
14. Fung, L. K., Shin, M., Tyler, B., Brem, H., and Saltzman, W. M. Chemotherapeutic drugs released from polymers: distribution of 1,3-bis(2-chloroethyl)-1-nitrosourea in the rat brain. Pharm. Res., *13:* 671–682, 1996.
15. Strasser, J. F., Fung, L. K., Eller, S., Grossman, S. A., and Saltzman, W. M. Distribution of 1,3-bis(2-chloroethyl)-1-nitrosourea (BCNU) and tracers in the rabbit brain after interstitial delivery by biodegradable polymer implants. J. Pharmacol. Exp. Ther. *275:* 1647–1655, 1995.
16. Grossman, S. A., Reinhard, C., Colvin, M., Chasin, M., Brundrett, R., Tamargo, R. J., and Brem, H. The intracerebral distribution of BCNU delivered by surgically implanted biodegradable polymers. J. Neurosurg., *76:* 640–647, 1992.
17. Domb, A. J., Rock, M., Schwartz, J., Perkin, C., Yipchuk, G., Broxup, B., and Villemure, J. G. Metabolic disposition and elimination studies of a radiolabelled biodegradable polymeric implant in the rat brain. Biomaterials, *15:* 681–688, 1994.
18. Buahin, K. G., Judy, K. D., Hartke, C., Domb, A. J., Maniar, M., Colvin, O. M., and Brem, H. Controlled release of 4-hydroperoxycyclophosphamide from the fatty acid dimer-sebacic acid copolymer. Polymers Adv. Technol., *3:* 311–316, 1992.
19. Zon, G., Ludeman, S. M., Brandt, J. A., Boyd, V. L., Ozkan, G., Egan, W., and Shao, K. L. NMR spectroscopic studies of intermediary metabolites of cyclophosphamide: a comprehensive kinetic analysis of the interconversion of *cis-* and *trans-*4-hydroxycyclophosphamide with aldophosphamide and the concomitant partitioning of aldophosphamide between irreversible fragmentation and reversible conjugation pathways. J. Med. Chem., *27:* 266–285, 1984.
20. Langer, R. Polymeric delivery systems for controlled drug release. Chem. Eng. Commun., *6:* 1–48, 1980.
21. Nicholson, C. Interaction between diffusion and Michaelis-Menten uptake of dopamine after ionophoresis in striatum. Biophys. J., *68:* 1699–1715, 1995.
22. Rosomoff, H. Method for simultaneous quantitative estimation of intracranial contents. J. Appl. Physiol., *16:* 395–396, 1961.
23. Wu, M. P., Tamada, J. A., Brem, H., and Langer, R. *In vivo versus in vitro* degradation of controlled release polymers for intracranial surgical therapy. J. Biomed. Materials Res., *28:* 387–395, 1994.
24. Leo, A., Hansch, C., and Elkins, D. Partition coefficients and their uses. Chem. Rev., *71:* 525–616, 1971.
25. Shabel, F. M., Johnston, T. P., McCaleb, G. S., Montgomery, J. A., Laster, W. R., and Skipper, H. E. Experimental evaluation of potential anti-cancer agents. VII. Effects of certain nitrosoureas on intracerebral L1210 leukemia. Cancer Res., *23:* 725–733, 1963.
26. Loo, T. L., Dixon, R. L., and Rall, D. P. The antitumor agent, 1,3-bis(2-chloroethyl)-1-nitrosourea. J. Pharm. Sci., *55:* 492–497, 1966.
27. Kanter, P. M., Schwartz, H. S., and West, C. R. Functional and chemical markers of PCNU activity. Cancer Drug Delivery, *1:* 11–20, 1983.
28. Blasberg, R. G., Patlak, C., and Fenstermacher, J. D. Intrathecal chemotherapy: brain tissue profiles after ventriculocisternal perfusion. J. Pharmacol. Exp. Ther., *195:* 73–83, 1975.
29. Reulen, H. J., Graham, R., Fenske, M., Tsuyumu, M., and Klatzo, I. The role of tissue pressure and bulk flow in the formation and resolution of cold-induced edema. *In:* H. M. Pappius and W. Feindel (ed.), Dynamics of Brain Edema, pp. 103–112. Berlin: Springer-Verlag, 1976.
30. Reulen, H. J., Graham, R., Spatz, M., and Klatzo, I. Role of pressure gradients and bulk flow in dynamics of vasogenic brain edema. J. Neurosurg., *46:* 24–35, 1977.

31. Reulen, H. J., Tsuyumu, M., Tack, A., Fenske, A. R., and Prioleau, G. R. Clearance of edema fluid into cerebrospinal fluid. J. Neurosurg., *48:* 754–764, 1978.
32. Yang, G. Y., Betz, A. L., Chenevert, T. L., Brunberg, J. A., and Hoff, J. T. Experimental intracerebral hemorrhage: relationship between brain edema, blood flow, and blood-brain barrier permeability in rats. J. Neurosurg., *81:* 93–102, 1994.
33. Ferszt, R., Neu, S., Cervos-Navarro, J., and Sperner, J. The spreading of focal brain edema induced by ultraviolet irradiation. Acta Neuropathol., *42:* 223–229, 1978.
34. Quencer, R. M., Post, M. J., and Hinks, R. S. Cine MR in the evaluation of normal and abnormal CSF flow: intracranial and intraspinal studies. Neuroradiology, *32:* 371–391, 1990.
35. Renkin, E. M. Cellular and intercellular transport pathways in exchange vessels. Am. Rev. Respir. Dis., *146:* S28–S31, 1992.
36. Jain, R. K. Determinants of tumor blood flow: a review. Cancer Res., *48:* 2641–2658, 1988.
37. Renkin, E. M. Transport pathways through capillary endothelium. Microvasc. Res., *15:* 123–135, 1978.
38. Renkin, E. M. Multiple pathways of capillary permeability. Circ. Res., *41:* 735–743, 1977.
39. Jaeger, C. B., Winn, S. R., Tresco, P. A., and Aebischer, P. Repair of the blood-brain barrier following implantation of polymer capsules. Brain Res., *551:* 163–170, 1991.
40. Oldfield, E. H., Dedrick, R. L., Chatterji, D. C., Yeager, R. L., Girton, M. E., Kornblith, P. L., and Doppman, J. L. Arterial drug infusion with extracorporeal removal. II. Internal carotid carmustine in rhesus monkeys. Cancer Treat. Rep., *69:* 293–303, 1985.
41. Henner, W. D., Peters, W. P., Eder, J. P., Antman, K., Schnipper, L., and Frei, E. Pharmacokinetics and immediate effects of high-dose carmustine in man. Cancer Treat. Rep., *70:* 877–880, 1986.
42. Shapiro, W. R., Grenn, S. B., Burger, P. C., Selker, R. G., VanGilder, J. C., Robertson, J. T., Mealey, J. J., Ransohoff, J., and Mahaley, M. S. A randomized comparison of intra-arterial *versus* intravenous BCNU, with or without intravenous 5-fluorouracil, for newly diagnosed patient with malignant glioma. J. Neurosurg., *76:* 772–781, 1992.
43. Fung, L. K., Ewend, M., Sills, A., Sipos, E., Thompson, R., Watts, M., Brem, H., and Saltzman, W. M. Carmustine distribution following Gliadel polymer implantation and interstitial release in the primate brain. *In:* First Scientific Meeting for the Society of Neuro-Oncology, Santa Fe, NM. Houston, TX: Society of Neuro-Oncology, 1996.
44. Fung, L. K., Hilton, J., Colvin, O. M., and Saltzman, W. M. Cytotoxic effects of low-dose, long-term exposure of BCNU in human glioma cells in culture. *In:* Second Annual Scientific Meeting for the Society for Neuro-Oncology, Charlottesville, VA. Houston, TX: Society of Neuro-Oncology, 1997.
45. Ketchum, R. E. B., and Gibson, D. M. Rapid isocratic reversed phase HPLC of taxanes on new columns developed specifically for Taxol analysis. J. Liquid Chromatogr., *16:* 2519–2530, 1993.
46. Levin, V. A., Hoffman, W., and Weinkam, R. J. Pharmacokinetics of BCNU in man: a preliminary study of 20 patients. Cancer Treat. Rep., *62:* 1305–1312, 1978.
47. Gerlowski, L. E., and Jain, R. Physiologically based pharmacological modeling: principles and applications (Review). J. Pharm. Sci., *72:* 1103–1127, 1983.
48. Levin, V. A. Relationship of octanol/water partition coefficient and molecular weight to rat brain capillary permeability. J. Med. Chem., *23:* 682–684, 1980.
49. Rapoport, S. I., Ohno, K., and Pettigrew, K. D. Drug entry into the brain. Brain Res., *172:* 354–359, 1979.
50. Rowinsky, E. K., Wright, M., Monsarrat, B., Lesser, G. J., and Donehower, R. C. Taxol: pharmacology, metabolism and clinical implications. Cancer Surv., *17:* 283–304, 1993.
51. Friedman, H. S., Colvin, O. M., Ludeman, S. M., Schold, S. C., Boyd, V. L., Mulhbaier, L. H., and Bigner, D. D. Experimental chemotherapy of human medulloblastoma with classical alkylators. Cancer Res., *46:* 2877–2833, 1986.
52. Heimans, J. J., Vermorken, J. B., Wolbers, J. G., Eeltink, C. M., Meijer, W. M., Taphoorn, M. J. B., and Beijnen, J. H. Paclitaxel (Taxol) concentrations in brain tumor tissue. Ann. Oncol., *5:* 951–953, 1994.
53. Arndt, C. A. S., Colvin, O. M., Balis, F. M., McCully, C. L., Johnston, G., and Poplack, D. G. Intrathecal administration of 4-hydroxycyclophosphamide in rhesus monkeys. Cancer Res., *47:* 5932–5934: 1987.
54. Kumar, G. N., Walle, U. K., Bhalla, K. N., and Walle, T. Binding of Taxol to human plasma, albumin and α_1-acid glycoprotein. Res. Commun. Chem. Pathol. Pharmacol., *80:* 337–344, 1993.
55. Scudiero, D. A., Meyer, S. A., Clatterbuck, B. E., Mattern, M. R., Ziolkowski, C. H., and Day, R. S. I. Sensitivity of human cell strains having different abilities to repair O^6-methylguanine in DNA to inactivation by alkylating agents including chloroethylnitrosoureas. Cancer Res., *44:* 2467–2474, 1984.
56. Domeyer, B. E., and Sladek, N. E. Kinetics of cyclophosphamide biotransformation *in vivo*. Cancer Res., *40:* 174–180, 1980.
57. Rahman, A., Korzekwa, K. R., Grogan, J., Gonzalez, F. J., and Harris, J. W. Selective biotransformation of Taxol to 6α-hydroxytaxol by human cytochrome P450 2C8. Cancer Res., *54:* 5543–5546, 1994.
58. Kumar, G., Ray, S., Walle, T., Haung, Y., Willingham, M., Self, S., and Bhalla, K. Comparative *in vitro* cytotoxic effects of Taxol and its major human metabolite 6α-hydroxytaxol. Cancer Chemother. Pharmacol., *36:* 129–135, 1995.
59. Pratt, W. B., Ruddon, R. W., Ensminger, W. D., and Maybaum, J. The Anticancer Drugs, Ed. 2, pp. 108–154. New York: Oxford University Press, 1994.
60. Hunter, K. J., Deen, D. F., Pellarin, M., and Marton, L. J. Effect of α-difluoromethylornithine on 1,3-bis(2-chloroethyl)-1-nitrosourea and *cis*-diamminedichloroplatinum(II) cytotoxicity, DNA interstrand cross-linking, and growth in human tumor cell lines *in vitro*. Cancer Res., *50:* 2769–2772, 1990.
61. Cahan, M. A., Walter, K. A., Colvin, O. M., and Brem, H. Cytotoxicity of Taxol *in vitro* against human and rat malignant tumors. Cancer Chemother. Pharmacol., *33:* 441–444, 1994.
62. Berne, R. M., and Levy, M. N. The arterial system. *In:* R. M. Berne and M. N. Levy (eds.), Physiology, pp. 486–507. St. Louis, MO: C. V. Mosby Co., 1988.
63. Wiedeman, M. P. Architecture. *In:* E. M. Renkin and C. C. Michel (eds.), The Cardiovascular System, Vol. IV, pp. 11–40. Bethesda, MD: American Physiological Society, 1984.
64. Rosenberg, G. A., Kyner, W. T., and Estrada, E. Bulk flow of brain interstitial fluid under normal and hyperosmolar conditions. Am. J. Physiol., *238:* F42–F49, 1980.